High-efficiency tomographic reconstruction of quantum states by quantum nondemolition measurements

J. S. Huang, L. F. Wei, and C. H. Oh

Phys. Rev. A **83**, 032110 — Published 14 March 2011

DOI: 10.1103/PhysRevA.83.032110

High efficiency tomographic reconstruction of quantum states by quantum nondemolition measurements

J. S. Huang,[1,2] L. F. Wei*,[1,3] and C. H. Oh†[2]

[1]*Quantum Optoelectronics Laboratory, School of Physics and Technology, Southwest Jiaotong University, Chengdu 610031, China*

[2]*Centre for Quantum Technologies and Department of Physics, National University of Singapore, 3 Science Drive 2, Singapore 117542, Singapore*

[3]*State Key Laboratory of Optoelectronic Materials and Technologies, School of Physics and Engineering, Sun Yat-Sen University Guangzhou 510275, China*

We propose a high efficiency scheme to tomographically reconstruct an unknown quantum state of the qubits, by using a series of quantum nondemolition (QND) measurements. The proposed QND measurements of the qubits are implemented by probing the stationary transmissions through a driven dispersively-coupled resonator. It is shown that only one kind of QND measurements is sufficient to determine all the diagonal elements of the density matrix of the detected quantum state. The remaining non-diagonal elements can be similarly determined by transferring them to the diagonal locations after a series of unitary operations. Compared with the tomographic reconstructions based on the usual destructive projective measurements (wherein one kind of such measurements can determine only one diagonal element of the density matrix), the present reconstructive approach exhibits significantly high efficiency. Specifically, our generic proposal is demonstrated by the experimental circuit quantum electrodynamics systems with a few Josephson charge qubits.

PACS number(s): 03.65.Wj, 42.50.Pq, 03.67.Lx, 85.25.Cp

I. INTRODUCTION

Reconstruction of an unknown quantum state by a series of quantum measurements is called quantum-state tomography [1], which is particularly important in the study of quantum mechanics and quantum information processing. Recently, many theoretical analysis and experimental demonstrations have been devoted to the implementations of the desirable quantum-state tomographies with, e.g., the polarized photons [2, 3], trapped ions [4], and the solid-state qubits [5], etc. Generally, to tomographically reconstruct a d-dimensional quantum state (corresponding to a $d \times d$ density matrix), one needs to determine $d^2 - 1$

* weilianfu@gmail.com
† phyohch@nus.edu.sg

real parameters by quantum measurements.

Usually, one kind of projective measurements (PMs), i.e., projecting the detected quantum system to one of the basis states, can be directly utilized to determine one of the diagonal elements of the density matrix. For instance, the current flowing through the SET is detected [6, 7] to read out the charge state $|1\rangle$ for directly determining the diagonal element $|1\rangle\langle 1|$ in the density matrix of the single charge qubit. Similarly, the diagonal element $|1\cdots 1\rangle\langle 1\cdots 1|$ of the N-qubit density matrix can be directly determined by the direct projection $\bigotimes_{l=0}^{N-1}(|1_l\rangle\langle 1_l|)$ (to the basis $|1\cdots 1\rangle$). Note that the directly projective setups in most experiments are fixed, additional quantum operations are thus required to beforehand transfer the other elements to the diagonal location for detections. Therefore, a series of quantum operations plus the direct projection (called as a series of PMs) are required to reconstruct the density matrix. Generally, d^2-1 kinds of PMs are required to determine d^2-1 independent parameters in the $d\times d$ density matrix. A typical example is that 15 kinds PMs are required to tomographically reconstruct an unknown two-qubit quantum state [5]. Here and thereinafter, one kind of PMs refers to the measurements either by the projective measurements to directly determine one diagonal element in the density matrix or by the measurements after the unitary operations used for transferring a non-diagonal element to that diagonal location.

The PMs utilized above must destroy the detected quantum state [7, 8]. Consequently, the fidelities of these measurements are usually limited by the inevitable back-action noises. Fortunately, besides the usual PMs, quantum state can also be detected by other strategies, typically such as the quantum nondemolition (QND) measurements. In these approaches other objects, rather than the dispersively-coupled qubits, are destructively measured. As a consequence the measurement-induced noises acting on the qubits could be effectively suppressed [9]. Therefore, QND measurements are practically regarded as the indirect but ideal PMs of the qubits.

Historically, QND measurements were proposed to explore the fundamental limitations of quantum measurements, and have been demonstrated in various fields of physics, such as the gravitational-wave detections [9], quantum optics [10–12], quantum controls [13], and the telecommunications [14], etc. In particular, the QND measurements have also been successfully applied to probe the atomic qubits in cavity quantum electrodynamics (QED) [15, 16], and the superconducting qubits in the circuit QEDs [17–23]. Specifically, the QND measurements demonstrated in circuit QEDs were implemented by measuring the transmissions of the microwave signals through the transmission line resonators. With such a strategy the qubit states can be read out by detecting the shifted frequencies of the resonator. This is because that different basis states of the qubit(s) cause different frequency-shifts of the resonator, and thus can be effectively distinguished.

Motivated by the above circuit-QED experiments, in a recent work we proposed a scheme to nondestructively detect the superposition of the basis states by the QND measurements [24]. Taking account of the full quantum correlations between

the cavity and dispersively-coupled qubit(s), we find that each of the basis states can be projected with a relevant probability. Therefore, the detected transmission spectra should reveal multiple peaks: each of them marks one of the basis states, and the relative height of such a peak is related to the probability of the corresponding basis state superposed in the detected state. Consequently, just one kind of the QND measurements can determine all the diagonal elements of the relevant density matrix. This is a manifest advantage over the usual PMs, wherein only one fixed basis was projected. Furthermore, by other kinds of QND measurements all the non-diagonal elements of the density matrix can then be determined, via performing certain suitable unitary operations to transfer them to the measurable diagonal locations. Since one kind of QND measurements can determine all the diagonal elements of the density matrix, the tomographic reconstruction based on such measurements should have significantly high efficiency, compared with the previous reconstructive approach based on the usual PMs.

The paper is organized as follows. Sec. II gives our generic model to describe the transmission of a driven resonator, and shows how to implement the tomographic reconstruction of a single-qubit state by the proposed QND measurements. The extension to the two-qubit case is given in Sec. III, where the advantage of our proposal over the previous tomographic reconstruction based on the usual PMs is apparent. Indeed, 6 kinds of QND measurements are sufficient to tomographically reconstruct a two-qubit state, while 15 kinds of PMs are required by the previous approach. The possible generalization to the N-qubit (with $N > 2$) case and summarization of our main results are finally given in Sec. IV.

II. TOMOGRAPHIC RECONSTRUCTION OF A SINGLE-QUBIT STATE BY QND MEASUREMENTS

For generality, we consider a cavity QED system consisting of N qubits. The Hamiltonian of the system reads

$$H = \hbar\omega_r \hat{a}^\dagger \hat{a} + \sum_{j=1}^{N} [\frac{\hbar\omega_j}{2}\sigma_{z_j} + \hbar g_j(\sigma_{+_j}\hat{a} + \sigma_{-_j}\hat{a}^\dagger)], \tag{1}$$

where $a^{(\dagger)}$ and $\sigma_{\pm_j}$ are ladder operators for the photon field and the jth qubit, respectively. Also, ω_r is the cavity frequency, ω_j the jth qubit transition frequency and g_j the coupling strength between the jth qubit and the resonator. The coherent drivings of the cavity can be described by

$$H_d = \hbar\epsilon(\hat{a}^\dagger e^{-i\omega_d t} + \hat{a}e^{i\omega_d t}), \tag{2}$$

with ϵ being the real amplitude and ω_d the frequency of the applied drivings.

Under the usual Born-Markov approximation, the dynamics of the whole system with dissipations and dephasings is described by the following master equation [25]

$$\begin{aligned} \dot{\varrho}_N &= -\frac{i}{\hbar}[H_N, \varrho_N] + \kappa\mathcal{D}[\hat{a}]\varrho_N + \sum_{j=1}^{N}\gamma_{1,j}\mathcal{D}[\sigma_{-_j}]\varrho_N + \sum_{j=1}^{N}\frac{\gamma_{\phi,j}}{2}\mathcal{D}[\sigma_{z_j}]\varrho_N, \\ H_N &= H + H_d. \end{aligned} \tag{3}$$

Here, ϱ_N is the reduced density operator and the dissipation superoperator is defined by $\mathcal{D}[A]\varrho_N = A\varrho_N A^\dagger - A^\dagger A\varrho_N/2 - \varrho_N A^\dagger A/2$. The parameters in the last three terms in Eq. (3), i.e., κ, $\gamma_{1,j}$, and $\gamma_{\phi,j}$, are the decay and dephasing rates of the cavity photons and the jth qubit, respectively.

In what follows, we begin with the master equation (3) to calculate the frequency-dependent transmission of the cavity, which is proportional to the steady-state mean photon number $\langle\hat{a}^\dagger\hat{a}\rangle$ in the cavity. Technically, to satisfy the basic criteria for the desirable QND measurements of the N-qubit system, the dispersive conditions

$$0 < \frac{g_j}{\Delta_j}, \frac{g_j g_{j'}}{\Delta_j \Delta_{jj'}}, \frac{g_j g_{j'}}{\Delta_{j'} \Delta_{jj'}} \ll 1, \ j \neq j' = 1, 2, ..., N \tag{4}$$

should be satisfied. These conditions assure also that the interbit interactions are negligible. In the above, $\Delta_j = \omega_j - \omega_r$ denotes the detuning between the jth qubit and the cavity, and $\Delta_{jj'} = \omega_j - \omega_j'$ the detuning between the jth and j'th qubits.

Below, we investigate the simplest case, wherein a single qubit with transition frequency ω_1 is dispersively coupled to the cavity mode, to explain the basic idea of our generic proposal.

A. Nondestructive detection of a single qubit by cavity transmissions

The Hamiltonian for the present simpler system reads ($\hbar = 1$ throughout the paper)

$$\tilde{H}_1 = \frac{\tilde{\omega}_1}{2}\sigma_{z_1} + (-\Delta_{dr} + \Gamma_1\sigma_{z_1})\hat{a}^\dagger\hat{a} + \epsilon(\hat{a}^\dagger + \hat{a}), \tag{5}$$

with the cavity-driving detuning $\Delta_{dr} = \omega_d - \omega_r$, $\tilde{\omega}_1 = \omega_1 + \Gamma_1$ and $\Gamma_1 = g_1^2/\Delta_1$. The corresponding master equation for the single-qubit plus the driven resonator takes the form

$$\dot{\varrho}_1 = -i[\tilde{H}_1, \varrho_1] + \kappa\mathcal{D}[\hat{a}]\varrho_1 + \gamma_{1,1}\mathcal{D}[\sigma_{-_1}]\varrho_1 + \frac{\gamma_{\phi,1}}{2}\mathcal{D}[\sigma_{z_1}]\varrho_1. \tag{6}$$

Obviously, the desirable quantity $\langle\hat{a}^\dagger\hat{a}\rangle$ can be determined by solving the following coupled equations of motion:

$$\frac{d\langle\hat{a}^\dagger\hat{a}\rangle}{dt} = -\kappa\langle\hat{a}^\dagger\hat{a}\rangle - 2\epsilon\mathrm{Im}\langle\hat{a}\rangle, \tag{7a}$$

$$\frac{d\langle\hat{a}\rangle}{dt} = (i\Delta_{dr} - \frac{\kappa}{2})\langle\hat{a}\rangle - i\Gamma_1\langle\hat{a}\sigma_{z_1}\rangle - i\epsilon, \tag{7b}$$

$$\frac{d\langle\hat{a}\sigma_{z_1}\rangle}{dt} = (i\Delta_{dr} - \frac{\kappa}{2} - \gamma_{1,1})\langle\hat{a}\sigma_{z_1}\rangle - (i\Gamma_1 + \gamma_{1,1})\langle\hat{a}\rangle - i\epsilon\langle\sigma_{z_1}\rangle, \tag{7c}$$

and

$$\frac{d\langle\sigma_{z_1}\rangle}{dt} = -\gamma_{1,1}(\langle\sigma_{z_1}\rangle + 1). \tag{7d}$$

One can see that the additional measurement-induced dephasing rate $\gamma_{\phi,1}$ does not influence the solutions of the equations. As the decay $\gamma_{1,1}$ of the qubit is significantly less than the decay rate κ of the driven cavity, the average of σ_{z_1} could be safely assumed to be unchanged during the detections. In fact, the characterized time of the detection is determined mainly by the decay of the cavity κ. Such a quantity is about $2\pi \times 1.69$ MHZ [22], which is obviously larger than $\gamma_{1,1} = 2\pi \times 0.02$ MHZ [19]. Experimentally, the time interval of completing a single QND detection is about $T_e = 40$ns [22], this is significantly shorter than the decoherence time $T_1 \sim 7.3\mu$s [19]. Therefore, during such a readout the decay of the qubit is really negligible, i.e., $\langle\sigma_{z_1}(T_e)\rangle = \exp(-\gamma_{1,1}T_e)(\langle\sigma_{z_1}(0)\rangle + 1) - 1 \approx \langle\sigma_{z_1}(0)\rangle$.

Under the steady-state conditions, we obtain

$$\begin{aligned}\frac{\langle\hat{a}^\dagger\hat{a}\rangle_{ss}}{\epsilon^2} &= \frac{2}{\kappa}[(\frac{\kappa}{2}+\gamma_{1,1})(\frac{\kappa^2}{4}+\frac{\gamma_{1,1}\kappa}{2}+\Gamma_1^2-\Delta_{dr}^2)+(\Delta_{dr}+\Gamma_1\langle\sigma_{z_1}(0)\rangle)(\kappa\Delta_{dr}+\gamma_{1,1}\Delta_{dr}+\gamma_{1,1}\Gamma_1)] \\ &\quad [(\frac{\kappa^2}{4}+\frac{\gamma_{1,1}\kappa}{2}+\Gamma_1^2-\Delta_{dr}^2)^2+(\kappa\Delta_{dr}+\gamma_{1,1}\Delta_{dr}+\gamma_{1,1}\Gamma_1)^2]^{-1}, \qquad (8)\end{aligned}$$

which is strongly related to the the initial state of the qubit.

The measured cavity transmissions (normalized to the peak height of the empty cavity (EMC) transmission) versus the probe frequency detunings are plotted in Fig. 1. Generally, the qubit is assumed to be prepared initially in the state $|\psi\rangle_1 = \beta_0|0\rangle+\beta_1|1\rangle$. Obviously, when $\beta_0 = 0$ (or 1), it reduces to the single basis state $|1\rangle$ (or $|0\rangle$). Compared with the empty cavity transmission (see Appendix), which is also plotted as the dark line in Fig. 1, one observes that the existence of the qubit leads to a right (left) shift of the single peak by a quantity $-\Gamma_1$ (Γ_1). This result is well agreement with the experimental observations in Refs. [17, 18]. This indicates that, the shifts of the peaks can be used to mark the basis states of the qubit. If the qubit is prepared at the superposition of the two basis states, e.g., $|\beta_1|^2 = 0.2, 0.4$, and 0.5, respectively, the spectra show the two-peak structures: the peak-locations coincide with that for the single basis states, but the relative heights of them correspond clearly to the superposed probabilities, i.e., $|\beta_0|^2$ and $|\beta_1|^2$, respectively.

Now, we discuss the physical mechanism why the above two-peak phenomenon can appear. Before applying the driving to detect the qubit, the qubit (prepared at the superposed state $\beta_0|0\rangle + \beta_1|1\rangle$) entangles to the pulled cavity. Roughly, the dispersive coupling Hamiltonian $\Gamma_1\sigma_{z_1}\hat{a}^\dagger\hat{a}$ generates an qubit-cavity entangled state $|0\rangle \otimes |f_0\rangle + |1\rangle \otimes |f_1\rangle$, with $|f_0\rangle$ and $|f_1\rangle$ being the cavity states (with the frequency shifts $-\Gamma_1$ and Γ_1, respectively). Since only the resonant incident photon can transmit the cavity, the cavity will be collapsed to either the state $|f_0\rangle$ or the state $|f_1\rangle$. Certainly, the probability of transmitting the photon with frequency shift $-\Gamma_1$ (or Γ_1) is $|\beta_0|^2$ (or $|\beta_1|^2$). After such a disentangled measurement process, the qubit would be collapsed to the state $|0\rangle$ (or the state $|1\rangle$). Experimentally, a number of measurements are performed on many copies of the detected state, and parts of them obtain the photon with the frequency shift $-\Gamma_1$ and others with the frequency shift Γ_1. This is why the two peaks can be observed statistically in the transmission spectra of the cavity. In the original definition of the

QND measurement, the measured operator (here σ_{z_1}) has the eigenstates that are also the eigenstates of the dispersive-coupling Hmiltonian. This means that the expectation value of the measured operator is conserved. Once the detector is projected to one of its eigenstates, the system is meanwhile collapsed to its relevant eigenstate. As a consequence, successive PMs give the same result as that obtained by the initial PM [26]. Similarly, in the measurements used in our work, decay of the detected resonator is dominant and the observables of the qubit operators are still conserved. Different eigenstates of the qubit operator pull the cavity with the different frequency shifts. Once the transmitted photon is detected, the frequency shift of the cavity is determined, and thus the qubit is collapsed to one of its basis states. Consequently, the sequential measurements after this detection must result in the same output. In this sense, the present measurements could also be regarded as the nondemolition ones, since their measurements are repeatable and all the subsequent measurements give exactly the same result as that obtained by the initial measurement.

B. Tomographic reconstruction of a single-qubit state

Above investigation indicates that partial information of the qubit state, i.e., the diagonal elements of the relevant density matrix, can be directly obtained by only one kind of the QND measurements. However, to extract the full information of an unknown qubit state, one should tomographically reconstruct all the elements of its density matrix. To completely define a d-dimensional density matrix ρ, one needs to determine d^2-1 real parameters.

Now we demonstrate how to perform the tomographic constructions of an arbitrary single-qubit state $|\psi\rangle_1 = \beta_0|0\rangle + \beta_1|1\rangle$ with the density matrix

$$\rho_1 = \begin{pmatrix} \rho_{00} & \rho_{01} \\ \rho_{10} & \rho_{11} \end{pmatrix}. \tag{9}$$

An efficient and widely used technique is to parameterize the density matrix ρ_1 on a Bloch sphere [5],

$$\rho_1 = \frac{1}{2}(I + \sum_{i=x,y,z} r_i\sigma_i) = \frac{1}{2}\begin{pmatrix} 1+r_z & r_x - ir_y \\ r_x + ir_y & 1-r_z \end{pmatrix}. \tag{10}$$

Here, I denotes the identity matrix, σ_i the Pauli matrices, and r_i real parameters. Therefore, in order to determine the single-qubit state, we must identify the three components (r_x, r_y, r_z) of the Bloch vector $\vec{r}$. As discussed in the previous section, two diagonal elements ρ_{00} and ρ_{11} can be directly determined by measuring the occupation probabilities $|\beta_0|^2$ and $|\beta_1|^2$. This means that the parameter r_z can be determined by the relation $r_z = \rho_{00} - \rho_{11} = |\beta_0|^2 - |\beta_1|^2$. To obtain the other two parameters r_x and r_y, we need to determine the non-diagonal elements. To this end, we perform the single-qubit operations $U_{x_1} = \exp(i\pi\sigma_{x_1}/4)$

and $U_{y_1} = \exp(i\pi\sigma_{y_1}/4)$ to transfer the left non-diagonal elements to the relevant diagonal locations. For example, after the operation U_{x_1}, the density matrix ρ_1 is changed to

$$\rho_1' = U_{x_1}\rho_1 U_{x_1}^\dagger = \frac{1}{2}\begin{pmatrix} 1-r_y & r_x - ir_z \\ r_x + ir_z & 1+r_y \end{pmatrix}. \tag{11}$$

Then performing another kind of QND measurements the parameters $|\beta_0'|^2$ and $|\beta_1'|^2$ are determined. Consequently, the coefficient r_y can be determined via the relation $r_y = |\beta_1'|^2 - |\beta_0'|^2$. Similarly, by performing the quantum operation U_{y_1} on the original density matrix ρ_1, another new density matrix

$$\rho_1'' = U_{y_1}\rho_1 U_{y_1}^\dagger = \frac{1}{2}\begin{pmatrix} 1+r_x & -r_z - ir_y \\ -r_z + ir_y & 1-r_x \end{pmatrix} \tag{12}$$

can be obtained, and the coefficient r_x is determined in the same way. Note that the number of the unitary operations required to implement the present tomographic reconstructions is the same as that required by the previous approach based on the usual PMs. Thus, for the single-qubit case the complexity of the present approach is the same as that in the previous one, and the efficiency is not enhanced.

The remaining task is to implement the single-qubit operations required above for transferring the non-diagonal elements to the diagonal locations. In a circuit-QED system, a superconducting charge qubit is strongly coupled to the transmission line resonator [17]. Following Ref. [27] and under a displacement transformation, the effective Hamiltonian of the resonator plus qubit system can be written as

$$\tilde{H} = -\Delta_{dr}\hat{a}^\dagger\hat{a} + \frac{\Delta_a}{2}\sigma_{z_1} + g_1(\hat{a}^\dagger\sigma_{-_1} + \hat{a}\sigma_{+_1}) + \frac{\Omega}{2}\sigma_{x_1}, \tag{13}$$

with the qubit-driving detuning $\Delta_a = \omega_1 - \omega_d$ and the Rabi frequency $\Omega = 2\epsilon g_1/(-\Delta_{dr})$. In the dispersive regime, i.e., $|g_1/\Delta_1| \ll 1$, and after the transformation $U_1 = \exp[-g_1(\hat{a}^\dagger\sigma_{-_1} - \hat{a}\sigma_{+_1})/\Delta_1]$, the above Hamiltonian becomes

$$H_x = -\Delta_{dr}\hat{a}^\dagger\hat{a} + \frac{\tilde{\Delta}_a}{2}\sigma_{z_1} + \frac{\Omega}{2}\sigma_{x_1}, \tag{14}$$

with $\tilde{\Delta}_a = \Delta_a + \Gamma_1$. First, if the condition $\tilde{\Delta}_a = 0$ is satisfied, then the Hamiltonian (14) produces a rotation of the qubit state about the x axis, i.e., U_{x_1} is generated by choosing the evolution time $t_x = \pi/(2\Omega)$. Second, if the driving is sufficiently detuned from the qubit, another approximate Hamiltonian

$$H_z = -\Delta_{dr}\hat{a}^\dagger\hat{a} + \frac{1}{2}(\tilde{\Delta}_a + \frac{1}{2}\frac{\Omega^2}{\Delta_a})\sigma_{z_1} \tag{15}$$

can be obtained by further performing a transformations $U_2 = \exp(\beta^*\sigma_{+_1} - \beta\sigma_{-_1})$, $\beta = \Omega/(2\Delta_a)$ on the Hamiltonian (14). Obviously, the desirable operation U_{z_1} can be implemented by the evolution under the Hamiltonian (15) with the duration $t_z = \pi\Delta_a/(2\Delta_a\tilde{\Delta}_a + \Omega^2)$. Third, the desirable operation U_{y_1} could be constructed as $U_{y_1} = \exp(i\pi\sigma_{y_1}/4) = \exp(i\pi\sigma_{z_1}/4)\exp(i3\pi\sigma_{x_1}/4)\exp(i3\pi\sigma_{z_1}/4)$. Finally, the duration t_x (or t_z) of the single-qubit operation required above is estimated as ~ 100ps with the experimental parameters: $\epsilon \sim 2\pi \times 20$MHz [21], and $\Delta_{dr} \sim \kappa/2$ [27]. This is significantly less by at least two orders than the qubit decoherence time, which is measured as $T_1 \sim 7.3\mu$s [19, 27]. Therefore, the required gate operations are accessible and the proposed tomographic reconstructions is experimentally feasible.

As an example, we assume that the three parameters $r_x = 0.5$, $r_y = \sqrt{2}/2$, $r_z = 0.5$ are obtained through the above reconstructions, then the reconstructed state can be written as $\rho_1 = 0.75|0\rangle\langle 0| + (0.25 - i\sqrt{2}/4)|0\rangle\langle 1| + (0.25 + i\sqrt{2}/4)|1\rangle\langle 0| + 0.25|1\rangle\langle 1|$, whose real $\rho_{ij}^{(R)}$ and imaginary $\rho_{ij}^{(I)}$ parts $(i, j = 0, 1)$ are graphically represented in Fig. 2.

III. TOMOGRAPHIC RECONSTRUCTION OF A TWO-QUBIT STATE BY QND MEASUREMENTS

A. Nondestructive detection of an unknown two-qubit state by cavity transmissions

In this section we extend the above single-qubit QND measurements to the two-qubit case. The transition frequencies of the two qubits are represented as ω_1 and ω_2, respectively. The effective Hamiltonian of the present system is

$$\tilde{H}_2 = (-\Delta_{dr} + \Gamma_1\sigma_{z_1} + \Gamma_2\sigma_{z_2})\hat{a}^\dagger\hat{a} + \frac{\tilde{\omega}_1}{2}\sigma_{z_1} + \frac{\tilde{\omega}_2}{2}\sigma_{z_2} + \epsilon(\hat{a}^\dagger + \hat{a}), \tag{16}$$

where $\Gamma_j = g_j^2/\Delta_j$ and $\tilde{\omega}_j = \omega_j + \Gamma_j$, $j = 1, 2$. Similarly, the relevant master equation reads

$$\dot{\varrho}_2 = -i[\tilde{H}_2, \varrho_2] + \kappa\mathcal{D}[\hat{a}]\varrho_2 + \sum_{j=1,2}\gamma_{1,j}\mathcal{D}[\sigma_{-_j}]\varrho_2 + \sum_{j=1,2}\frac{\gamma_{\phi,j}}{2}\mathcal{D}[\sigma_{z_j}]\varrho_2 \tag{17}$$

and the equations of motion for the mean values of various expectable operators are

$$\frac{d\langle\hat{a}^\dagger\hat{a}\rangle}{dt} = -\kappa\langle\hat{a}^\dagger\hat{a}\rangle - 2\epsilon\mathrm{Im}\langle\hat{a}\rangle, \tag{18a}$$

$$\frac{d\langle\hat{a}\rangle}{dt} = (i\Delta_{dr} - \frac{\kappa}{2})\langle\hat{a}\rangle - i\Gamma_1\langle\hat{a}\sigma_{z_1}\rangle - i\Gamma_2\langle\hat{a}\sigma_{z_2}\rangle - i\epsilon, \tag{18b}$$

$$\frac{d\langle\hat{a}\sigma_{z_1}\rangle}{dt} = (i\Delta_{dr} - \frac{\kappa}{2} - \gamma_{1,1})\langle\hat{a}\sigma_{z_1}\rangle - (i\Gamma_1 + \gamma_{1,1})\langle\hat{a}\rangle - i\Gamma_2\langle\hat{a}\sigma_{z_1}\sigma_{z_2}\rangle - i\epsilon\langle\sigma_{z_1}\rangle, \tag{18c}$$

$$\frac{d\langle\hat{a}\sigma_{z_2}\rangle}{dt} = (i\Delta_{dr} - \frac{\kappa}{2} - \gamma_{1,2})\langle\hat{a}\sigma_{z_2}\rangle - (i\Gamma_2 + \gamma_{1,2})\langle\hat{a}\rangle - i\Gamma_1\langle\hat{a}\sigma_{z1}\sigma_{z_2}\rangle - i\epsilon\langle\sigma_{z_2}\rangle, \tag{18d}$$

$$\frac{d\langle\hat{a}\sigma_{z_1}\sigma_{z_2}\rangle}{dt} = (i\Delta_{dr}-\frac{\kappa}{2}-\gamma_{1,1}-\gamma_{1,2})\langle\hat{a}\sigma_{z_1}\sigma_{z_2}\rangle - i\epsilon\langle\sigma_{z_1}\sigma_{z_2}\rangle - (i\Gamma_2+\gamma_{1,2})\langle\hat{a}\sigma_{z_1}\rangle - (i\Gamma_1+\gamma_{1,1})\langle\hat{a}\sigma_{z_2}\rangle, \tag{18e}$$

$$\frac{d\langle\sigma_{z_1}\rangle}{dt} = -\gamma_{1,1}(\langle\sigma_{z_1}\rangle+1), \tag{18f}$$

$$\frac{d\langle\sigma_{z_2}\rangle}{dt} = -\gamma_{1,2}(\langle\sigma_{z_2}\rangle+1), \tag{18g}$$

$$\frac{d\langle\sigma_{z_1}\sigma_{z_2}\rangle}{dt} = -(\gamma_{1,1}+\gamma_{1,2})\langle\sigma_{z_1}\sigma_{z_2}\rangle - \gamma_{1,1}\langle\sigma_{z_2}\rangle - \gamma_{1,2}\langle\sigma_{z_1}\rangle. \tag{18h}$$

Likewise, due to the relatively-long decoherence time of the qubits and their sufficiently short measurement time, the influences of the additional measurement-induced dephasing and decays of the qubits are also unimportant. Thus, the expectation values of the qubit operators can still be regarded as unchanged, i.e., $\langle\sigma_{z_j}(t)\rangle \approx \langle\sigma_{z_j}(0)\rangle$ and $\langle\sigma_{z_1}(t)\sigma_{z_2}(t)\rangle \approx \langle\sigma_{z_1}(0)\sigma_{z_2}(0)\rangle$, during the QND measurements. As a consequence, one can easily solve the above Eqs. (18a-e) and finally obtain the exact steady-state distributions of the intracavity photon number

$$\frac{\langle\hat{a}^\dagger\hat{a}\rangle_{ss}}{\epsilon^2} = \frac{2}{\kappa}\mathrm{Re}\left\{\frac{F(\sum_{j,j'}B_jD_{j'}G_j+D_1D_2)+B_1B_2[G_{12}(D_1+D_2)+\sum_{j,j'}E_jG_{j'}]-\sum_j B_jE_j(D_j+B_jG_j)}{\sum_{j,j'}B_jE_j(D_{j'}F+D_jA)-(B_1E_1-B_2E_2)^2-AD_1D_2F}\right\}, \quad j,j'=1,2,j\neq j'. \tag{19}$$

Here, $A=i\Delta_{dr}-\kappa/2, B_j=i\Gamma_j, D_j=i\Delta_{dr}-\kappa/2-\gamma_{1,j}, E_j=i\Gamma_j+\gamma_{1,j}, F=i\Delta_{dr}-\kappa/2-\gamma_{1,1}-\gamma_{1,2}$, $G_j=\langle\sigma_{z_j}(0)\rangle$, and $G_{12}=\langle\sigma_{z_1}(0)\sigma_{z_2}(0)\rangle$.

We now investigate the above distributions schematically for various two-qubit states expressed by $|\psi\rangle_2=\alpha_1|00\rangle+\alpha_2|01\rangle+\alpha_3|10\rangle+\alpha_4|11\rangle$. First, we assume that the two-qubit is initially prepared at only one of the four basis states, i.e., only one of the four probability amplitudes equals 1. For this case Fig. 3 clearly shows that single peaks reveal, and these peaks can be well distinguished by the shifts of the central frequencies of the transmission spectra. In practical, the peaks with frequency shifts $-\Gamma_1-\Gamma_2$, $-\Gamma_1+\Gamma_2$, $\Gamma_1-\Gamma_2$, and $\Gamma_1+\Gamma_2$ mark respectively the state $|00\rangle$, $|01\rangle$, $|10\rangle$, and $|11\rangle$. These results are well agreement with the observations in Ref. [23], and clearly indicate that the pulls of the cavity strongly depend on the states of the qubits. Also, the relative heights of all these single peaks are exactly equivalent to 1, which is the same height as that for the EMC case.

Typically, if the two-qubit is prepared at the superposition of the four basis states, then the situations are quite different. It is seen from Fig. 3(a) that, if the two-qubit is prepared initially as one of the Bell states, i.e., $(|\alpha_1|^2, |\alpha_2|^2, |\alpha_3|^2, |\alpha_4|^2) =$

$(0.5, 0, 0, 0.5)$, then the transmitted spectrum of the cavity reveals two peaks with the same relative height 0.5. The locations of these two peaks are at the same positions for the states $|00\rangle$ and $|11\rangle$, respectively. Furthermore, for a more generic superposed state $(|\alpha_1|^2,\ |\alpha_2|^2,\ |\alpha_3|^2,\ |\alpha_4|^2) = (0.1, 0.2, 0.3, 0.4)$, four peaks reveal: the central positions of these peaks locate at the corresponding positions of basis states $|00\rangle, |01\rangle, |10\rangle$, and $|11\rangle$, respectively. The relative heights of these four peaks are $0.1, 0.212, 0.308$, and 0.4, respectively. Note that the relative heights of the peaks marking the states $|00\rangle$ and $|11\rangle$ are exactly equivalent to the superposed probabilities $|\alpha_1|^2$ and $|\alpha_4|^2$, respectively. While, the relative heights of the peaks marking the states $|01\rangle$ and $|10\rangle$ deviate from the corresponding superposed probabilities $|\alpha_2|^2$ and $|\alpha_3|^2$. This is because the two neighboring peaks are not well distinguished due to their partial overlap. In Fig. 3 (b) we modify the relevant parameters as $\Gamma_1' = 1.05\Gamma_1$ and $\Gamma_2' = 0.85\Gamma_2$, and then find that each of the four peaks is well separated from the others. In this case the relative height of each peak equals exactly to the expectable superposed probability of the corresponding basis state in the superposed state.

B. High efficiency tomographic reconstructions of a two-qubit state

The two-qubit state tomography can be done in the similar way as that for the above single-qubit state. Now, there are 15 real parameters to be determined for reconstructing a 4-dimensional density matrixρ_2. Generally, the 4-dimensional density matrix for a two-qubit state $|\psi\rangle_2 = \alpha_1|00\rangle + \alpha_2|01\rangle + \alpha_3|10\rangle + \alpha_4|11\rangle$ can be presented as

$$\rho_2 = \begin{pmatrix} \rho_{11} & \rho_{12} & \rho_{13} & \rho_{14} \\ \rho_{21} & \rho_{22} & \rho_{23} & \rho_{24} \\ \rho_{31} & \rho_{32} & \rho_{33} & \rho_{34} \\ \rho_{41} & \rho_{42} & \rho_{43} & \rho_{44} \end{pmatrix}, \tag{20}$$

in the bases: $\{|1\rangle_2 = |00\rangle, |2\rangle_2 = |01\rangle, |3\rangle_2 = |10\rangle, |4\rangle_2 = |11\rangle\}$. It can also be rewritten as [5]

$$\rho_2 = \frac{1}{4}\sum_{m,n=0,x,y,z} r_{mn}\sigma_{m_1}\otimes\sigma_{n_2} = \frac{1}{4}\begin{pmatrix} r_{00}+r_{0z}+r_{z0}+r_{zz} & r_{0x}+r_{zx}-ir_{0y}-ir_{zy} & r_{x0}+r_{xz}-ir_{y0}-ir_{yz} & r_{xx}-r_{yy}-ir_{xy}-ir_{yx} \\ r_{0x}+r_{zx}+ir_{0y}+ir_{zy} & r_{00}-r_{0z}+r_{z0}-r_{zz} & r_{xx}+r_{yy}+ir_{xy}-ir_{yx} & r_{x0}-r_{xz}-ir_{y0}+ir_{yz} \\ r_{x0}+r_{xz}+ir_{y0}+ir_{yz} & r_{xx}+r_{yy}-ir_{xy}+ir_{yx} & r_{00}+r_{0z}-r_{z0}-r_{zz} & r_{0x}-r_{zx}-ir_{0y}+ir_{zy} \\ r_{xx}-r_{yy}+ir_{xy}+ir_{yx} & r_{x0}-r_{xz}+ir_{y0}-ir_{yz} & r_{0x}-r_{zx}+ir_{0y}+ir_{zy} & r_{00}-r_{0z}-r_{z0}+r_{zz} \end{pmatrix}. \tag{21}$$

Here, $\sigma_{m=x,y,z}$ are the Pauli operators, σ_0 is identity matrix, and sixteen real parameters r_{mn} are to be determined. Note that the first and second subscripts of the matrix elements ρ_{ij} $(i,j=1,2,3,4)$ in Eq. (20) and r_{mn} in Eq. (21) are labeled for the first and second qubit, respectively.

As in the above discussions, performing the QND measurements on the two-qubit state can directly determine all the four diagonal elements ρ_{11}, ρ_{22}, ρ_{33} and ρ_{44}, by the measured results $|\alpha_1|^2$, $|\alpha_2|^2$, $|\alpha_3|^2$ and $|\alpha_4|^2$, respectively. As a consequence, the parameters r_{00}, r_{0z}, r_{z0} and r_{zz} can be determined by

$$\begin{aligned} r_{00} &= |\alpha_1|^2+|\alpha_2|^2+|\alpha_3|^2+|\alpha_4|^2=1, \\ r_{0z} &= |\alpha_1|^2-|\alpha_2|^2+|\alpha_3|^2-|\alpha_4|^2, \\ r_{z0} &= |\alpha_1|^2+|\alpha_2|^2-|\alpha_3|^2-|\alpha_4|^2, \\ r_{zz} &= |\alpha_1|^2-|\alpha_2|^2-|\alpha_3|^2+|\alpha_4|^2. \end{aligned} \tag{22}$$

To determine the other 12 parameters, we need to perform certain unitary operations to transfer them to the diagonal locations for other QND measurements.

It is well known that arbitrary two-qubit operation assisted by arbitrary rotations of the single qubits can generate an universal set of quantum gates. So, the key to implement the above required operations for quantum state tomography is to realize a two-qubit gate. For the experimental circuit QED system with two superconducting charge qubits, such a gate could be implemented by using the so-called FLICFORQ protocol [27]. In fact, if the cavity is driven by two external fields satisfying the sideband matching condition: $\omega_{d_2}-\omega_{d_1}=\Omega_1+\Omega_2$, an effective Hamiltonian

$$\tilde{H}_{\rm FF}=\omega_r\hat{a}^\dagger\hat{a}+\frac{g_1g_2(\Delta_1'+\Delta_2')}{16\Delta_1'\Delta_2'}(\sigma_{y_1}\otimes\sigma_{y_2}+\sigma_{z_1}\otimes\sigma_{z_2}) \tag{23}$$

can be induced in a quadruply rotating framework. Here, $\Delta_j'=\omega_{_j}+2\Omega_{jj'}^2/\Delta_{_{jdj'}}-\omega_r$, with $\Omega_{jj'}=2g_j\epsilon_{j'}/(\omega_{d_{j'}}-\omega_r)$ and $\Delta_{_{jdj'}}=\omega_{_j}-\omega_{d_{j'}}$, $j,j'=1,2$, $j\neq j'$. Obviously, the evolution under the above Hamiltonian with the duration, e.g., around 100ps for the experimental parameters [27], can produce a two-qubit operation

$$U_{\rm FF}=\exp[i\pi(\sigma_{y_1}\otimes\sigma_{y_2}+\sigma_{z_1}\otimes\sigma_{z_2})/4]. \tag{24}$$

On the other hand, the typical single-qubit gates U_{x_j}, U_{y_j} and U_{z_j} $(j=1,2)$ can be relatively easy to produce by using the similar approaches presented in Sec. II. With such a two-qubit operation and other single-qubit gates, we show how to perform the desirable unitary operations for transferring the non-diagonal elements to the diagonal locations in the table. For example, by performing a selected operational sequence $W=U_{\rm FF}U_{x_1}$ on the original density matrix ρ_2, we have a density matrix

$\rho_2' = W\rho_2 W^\dagger$, and the new diagonal elements are

$$\begin{aligned}
\rho_{11}' &= \frac{1}{4}(r_{00} + r_{xy} - r_{yz} + r_{zx}),\\
\rho_{22}' &= \frac{1}{4}(r_{00} + r_{xy} + r_{yz} - r_{zx}),\\
\rho_{33}' &= \frac{1}{4}(r_{00} - r_{xy} + r_{yz} + r_{zx}),\\
\rho_{44}' &= \frac{1}{4}(r_{00} - r_{xy} - r_{yz} - r_{zx}).
\end{aligned} \tag{25}$$

By the QND measurements the values of $|\alpha_1'|^2, |\alpha_2'|^2$, $|\alpha_3'|^2$, and $|\alpha_4'|^2$ are given. Consequently, the desirable parameters r_{00}, r_{xy}, r_{yz} and r_{zx} are obtained by the relations

$$\begin{aligned}
r_{00} &= |\alpha_1'|^2 + |\alpha_2'|^2 + |\alpha_3'|^2 + |\alpha_4'|^2 = 1,\\
r_{xy} &= |\alpha_1'|^2 + |\alpha_2'|^2 - |\alpha_3'|^2 - |\alpha_4'|^2,\\
r_{yz} &= -|\alpha_1'|^2 + |\alpha_2'|^2 + |\alpha_3'|^2 - |\alpha_4'|^2,\\
r_{zx} &= |\alpha_1'|^2 - |\alpha_2'|^2 + |\alpha_3'|^2 - |\alpha_4'|^2.
\end{aligned} \tag{26}$$

Similarly, other non-diagonal elements can also be determined. Note that here only six kinds of QND measurements are sufficient to tomographically reconstruct a two-qubit state. This is obviously simpler than the previous tomography based on the usual PMs, wherein 15 kinds of measurements are required [5, 23]. Thus, the present tomography is essentially high efficient.

After performing all the QND measurements listed in the table, a two-qubit state can be completely reconstructed. For example, six kinds of QND measurements can determine these parameters

$$\begin{pmatrix} r_{00} & r_{0x} & r_{0y} & r_{0z} \\ r_{x0} & r_{xx} & r_{xy} & r_{xz} \\ r_{y0} & r_{yx} & r_{yy} & r_{yz} \\ r_{z0} & r_{zx} & r_{zy} & r_{zz} \end{pmatrix} = \begin{pmatrix} 1 & 0 & 0 & -0.2 \\ 0 & 0.25 & 0 & 0.6 \\ 0 & 0 & -0.25 & 0 \\ -0.4 & 0.125 & 0 & 0 \end{pmatrix}, \tag{27}$$

then a two-qubit state can be effectively reconstructed by the following representation

$$\rho_2 = \begin{pmatrix} \rho_{11} & \rho_{12} & \rho_{13} & \rho_{14} \\ \rho_{21} & \rho_{22} & \rho_{23} & \rho_{24} \\ \rho_{31} & \rho_{32} & \rho_{33} & \rho_{34} \\ \rho_{41} & \rho_{42} & \rho_{43} & \rho_{44} \end{pmatrix}$$
$$= \begin{pmatrix} 0.1 & 0.0313 - i0.0313 & 0.15 - i0.15 & -i0.125 \\ 0.0313 + i0.0313 & 0.2 & 0.125 & -0.15 + i0.15 \\ 0.15 + i0.15 & 0.125 & 0.3 & -0.0313 + i0.0313 \\ i0.125 & -0.15 - i0.15 & -0.0313 + i0.0313 & 0.4 \end{pmatrix}. \quad (28)$$

The simulated reconstruction is graphically shown in Fig. 4, where $\rho_{ij}^{(R)}$ and $\rho_{ij}^{(I)}$ are the real and imaginary parts of the reconstructed state in the complete bases $|1\rangle_2 = |00\rangle$, $|2\rangle_2 = |01\rangle$, $|3\rangle_2 = |10\rangle$, $|4\rangle_2 = |11\rangle$, with $i, j = 1, 2, 3, 4$.

IV. DISCUSSIONS AND CONCLUSIONS

Generally, the quantum state tomographic constructions demonstrated above can be extended to the case including N ($N > 2$) qubits in a straightforward manner. This is because that the proposed QND measurements can be directly applied to determine all the diagonal elements of the arbitrary N-qubit state; various basis states can be inferred from the relevant positions of the measured peaks, and the probabilities of the corresponding bases superposed in the measured state can be extracted from the relative heights of the peaks (if they are sufficiently separated from the others). Moreover, all the required operations for the tomographic reconstructions can be implemented from the universal set of the gates. Thus, the efficiency of the tomographic reconstruction of the multi-qubit should be greatly improved by using the proposed QND measurements.

Note that the family of QND measurements (which are constructed by certain operational sequences) listed in the above table is not unique, and the other sets of measurements can also be used to do the desirable tomography. Hence, some parameters can be determined by different kinds of QND measurements. This property can be utilized to check the accuracy of the designed quantum operations. We also emphasize that the practically-existing decays of the qubits are safely-neglected in our treatments. The validity of these neglects depends on three parameters: the duration T_e for obtaining an experimental data of cavity transmission, the cavity decay time $T_c = 1/\kappa$ and the decay time $T_{1,j} = 1/\gamma_{1,j}$ of the detected qubits. The so-called steady-state transmission condition implies that $T_e \sim T_c$ is in the same order of around tens of nanoseconds. As the qubit decay is practically very slow, e.g., $T_1 = 7.3\mu$s [19], neglecting the effect from the qubit decays should be reasonable.

In summary, we have proposed a scheme to perform the quantum state tomography by the QND measurements. Detailed operations for reconstructing single- and two-qubit states are presented, respectively. Similarly, the proposal can be directly generalized to the multi-qubit case. Differing from the usual tomography based on the PMs, our reconstruction is based on a series of QND measurements. Since all the diagonal elements of the density matrix of an unknown quantum state can be determined by a single kind of the QND measurements, the efficiency of the present tomographic reconstruction is significantly higher for multiple qubits. Specifically, our proposal is demonstrated with the current circuit QED setups with a few charge qubits, and could also be generalized to other qubit-systems, at least in principle.

Acknowledgments

This work was supported in part by the National Science Foundation grant No. 10874142, 90921010, and the National Fundamental Research Program of China through Grant No. 2010CB923104, and the Fundamental Research Funds for the Central Universities No. SWJTU09CX078, and A*STAR of Singapore under research grant No. WBS: R-144-000-189-305.

APPENDIX: TRANSMISSION OF A DRIVEN EMPTY CAVITY

In this appendix, the transmission of a driven empty cavity is calculated. The Hamiltonian of the simplified system reduces to

$$H_0 = \omega_r \hat{a}^\dagger \hat{a} + \epsilon(\hat{a}^\dagger e^{-i\omega_d t} + \hat{a} e^{i\omega_d t}). \tag{A1}$$

After performing the time-dependent unitary transformation defined by the operator $R = \exp(-i\omega_d t \hat{a}^\dagger \hat{a})$, we get the effective Hamiltonian

$$\tilde{H}_0 = R^\dagger H_0 R - iR^\dagger \partial R/\partial t = -\Delta_{dr} \hat{a}^\dagger \hat{a} + \epsilon(\hat{a}^\dagger + \hat{a}), \tag{A2}$$

where $\Delta_{dr} = \omega_d - \omega_r$ is the detuning of the cavity from the driving. Then we get the master equation for such a driven empty cavity

$$\dot{\varrho}_0 \;=\; -i[\tilde{H}_0, \varrho_0] + \kappa(\hat{a}\varrho_0\hat{a}^\dagger - \hat{a}^\dagger\hat{a}\varrho_0/2 - \varrho_0\hat{a}^\dagger\hat{a}/2), \tag{A3}$$

where ϱ_0 is the density matrix of the empty cavity.

From the above master equation, one can easily obtain the equations of motion for the expectation values of the relevant operators, such as mean photon number inside the cavity $\langle \hat{a}^\dagger \hat{a} \rangle = \mathrm{Tr}(\hat{a}^\dagger \hat{a} \varrho_0)$:

$$\frac{d\langle \hat{a}^\dagger \hat{a} \rangle}{dt} \;=\; -\kappa \langle \hat{a}^\dagger \hat{a} \rangle - 2\epsilon \mathrm{Im}\langle \hat{a} \rangle, \tag{A4a}$$

with

$$\frac{d\langle\hat{a}\rangle}{dt} = (i\Delta_{dr} - \frac{\kappa}{2})\langle\hat{a}\rangle - i\epsilon. \tag{A4b}$$

The steady-state solution of Eq. (A4a) gives

$$\frac{\langle\hat{a}^\dagger\hat{a}\rangle_{ss}}{\epsilon^2} = \frac{1}{(\omega_d - \omega_r)^2 + (\frac{\kappa}{2})^2}. \tag{A5}$$

Obviously, the transmission spectrum of an empty cavity, which is proportional to $\langle\hat{a}^\dagger\hat{a}\rangle$, is the well-known Lorentzian: centered at $\omega_d = \omega_r$ with the half-width κ. When ω_d does not sufficiently match the cavity frequency, no photon penetrates the cavity and thus no transmission is recorded.

[1] M. G. A. Paris and J. Řeháček, *Quantum State Estimation*, Lect. Not. Phys. Vol. 649 (Springer, Berlin, 2004)

[2] A. G. White, D. F. V. James, P. H. Eberhard, and P. G. Kwiat, Phys. Rev. Lett. **83**, 3103 (1999)

[3] N. K. Langford, R. B. Dalton, M. D. Harvey, J. L. O'Brien, G. J. Pryde, A. Gilchrist, S. D. Bartlett, and A. G. White, Phys. Rev. Lett. **93**, 053601 (2004)

[4] H. Häffner, W. Hänsel, C. F. Roos, J. Benhelm, D. C. al kar, M. Chwalla, T. Körber, U. D. Rapol, M. Riebe, P. O. Schmidt, C. Becher, O. Gühne, W. Dür, and R. Blatt, Nature **438**, 643 (2005)

[5] Yu-xi Liu, L. F. Wei, and F. Nori, Europhys. Lett. **67**, 874 (2004); Yu-xi Liu, L. F. Wei, and F. Nori, Phys. Rev. B **72**, 014547 (2005)

[6] Y. A. Pashkin, T. Yamamoto, O. Astafiev, Y. Nakamura, D. V. Averin, and J. S. Tsai, Nature (London) **421**, 823 (2003); O. Astafiev, Y. A. Pashkin, T. Yamamoto, Y. Nakamura, and J. S. Tsai, Phys. Rev. B **69**, 180507 (2004)

[7] Y. Makhlin, G. Schön, and A. Shnirman, Rev. Mod. Phys. **73**, 357 (2001)

[8] D. Leibfried, R. Blatt, C. Monroe, and D. Wineland, Rev. Mod. Phys. **75**, 281 (2003); Ch. Raab, J. Eschner, J. Bolle, H. Oberst, F. Schmidt-Kaler, and R. Blatt, Phys. Rev. Lett. **85**, 538 (2000)

[9] V. B. Braginsky and F. Ya. Khalili, Rev. Mod. Phys. **68**, 1 (1996)

[10] S. F. Pereira, Z. Y. Ou, and H. J. Kimble, Phys. Rev. Lett. **72**, 214 (1994)

[11] K. Bencheikh, J. A. Levenson, Ph. Grangier, and O. Lopez, Phys. Rev. Lett. **75**, 3422 (1995)

[12] P. Grangier, J. A. Levenson and J. P. Poizat Nature (London) **396**, 537 (1998)

[13] H. M. Wiseman, Phys. Rev. A **51**, 2459 (1995)

[14] J. A. Levenson, I. Abram, T. Rivera, P. Fayolle, J. C. Garreau, and P. Grangier, Phys. Rev. Lett. **70**, 267 (1993)

[15] G. Nogues, A. Rauschenbeutel, S. Osnaghi, M. Brune, J. M. Raimond, and S. Haroche, Nature (London) **400**, 239 (1999)

[16] Q. A. Turchette, C. J. Hood, W. Lange, H. Mabuchi, and H. J. Kimble, Phys. Rev. Lett. **75**, 4710 (1995)

[17] A. Blais, R. S. Huang, A. Wallraff, S. M. Girvin, and R. J. Schoelkopf, Phys. Rev. A **69**, 062320 (2004)

[18] A. Wallraff, D. I. Schuster, A. Blais, L. Frunzio, R. S. Huang, J. Majer, S. Kumar, S. M. Girvin, and R. J. Schoelkopf, Nature (London) **431**, 162 (2004)

[19] A. Wallraff, D. I. Schuster, A. Blais, L. Frunzio, J. Majer, M. H. Devoret, S. M. Girvin, and R. J. Schoelkopf, Phys. Rev. Lett. **95**, 060501 (2005)

[20] L. F. Wei, Yu-xi Liu, C. P. Sun, and Franco Nori, Phys. Rev. Lett. **97**, 237201 (2006)

[21] J. Gambetta, A. Blais, M. Boissonneault, A. A. Houck, D. I. Schuster, and S. M. Girvin, Phys. Rev. A **77**, 012112 (2008)

[22] R. Bianchetti, S. Filipp, M. Baur, J. M. Fink, M. Göppl, P. J. Leek, L. Steffen, A. Blais, and A. Wallraff, Phys. Rev. A **80**, 043840 (2009)

[23] S. Filipp, P. Maurer, P. J. Leek, M. Baur, R. Bianchetti, J. M. Fink, M. Göppl, L. Steffen, J. M. Gambetta, A. Blais, and A. Wallraff, Phys. Rev. Lett. **102**, 200402 (2009)

[24] L. F. Wei, J. S. Huang, X. L. Feng, Z. D. Wang and C. H. Oh, arXiv: 1005. 2470

[25] D. F. Walls and G. J. Milburn, *Quantum Optics* (Spinger-Verlag, Berlin, 1994)

[26] J. Gambetta, W. A. Braff, A. Wallraff, S. M. Girvin, and R. J. Schoelkopf, Phys. Rev. A **76**, 012325 (2007)

[27] A. Blais, J. Gambetta, A. Wallraff, D. I. Schuster, S. M. Girvin, M. H. Devoret, and R. J. Schoelkopf, Phys. Rev. A **75**, 032329 (2007)

Figures

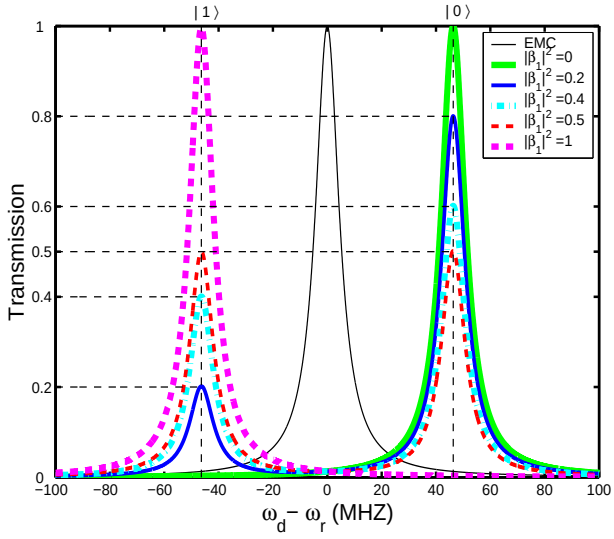

FIG. 1: (Color online) Cavity transmission for the single-qubit states versus the probe detuning $\omega_d - \omega_r$. Five cases of the qubit states for $|\beta_1|^2 = 0, 0.2, 0.4, 0.5$, and 1 are shown. For comparison, the empty cavity (EMC) transmission is also plotted in black line. The peak shifts by $-\Gamma_1$ or Γ_1 correspond to single basis state $|0\rangle$ or $|1\rangle$. For the superposition states, the double-peak relative heights (in contrast to the peak height of the empty cavity transmission) present clearly the superposed probabilities of the two basis states. Here, the parameters are selected as $(\Gamma_1, \kappa, \gamma_{1,1}) = 2\pi \times (-7.38, 1.69, 0.02)$MHz [19, 22].

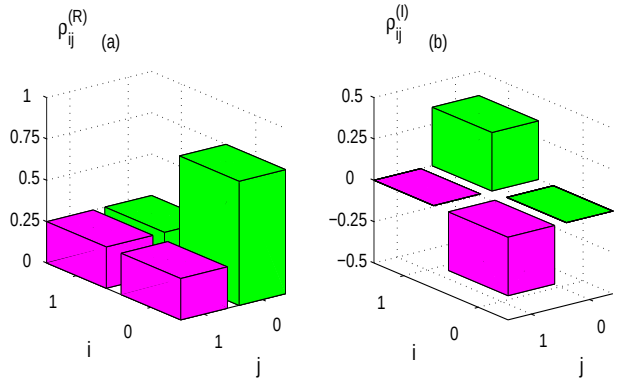

FIG. 2: (Color online) Graphic representations of the density matrix ρ_1 for a single-qubit state. The real $\rho_{ij}^{(R)}$ and imaginary $\rho_{ij}^{(I)}$ parts of the density matrix elements $\rho_{ij} = \langle i|\rho|j\rangle$ $(i, j = 0, 1)$ are plotted in (a) and (b), respectively.

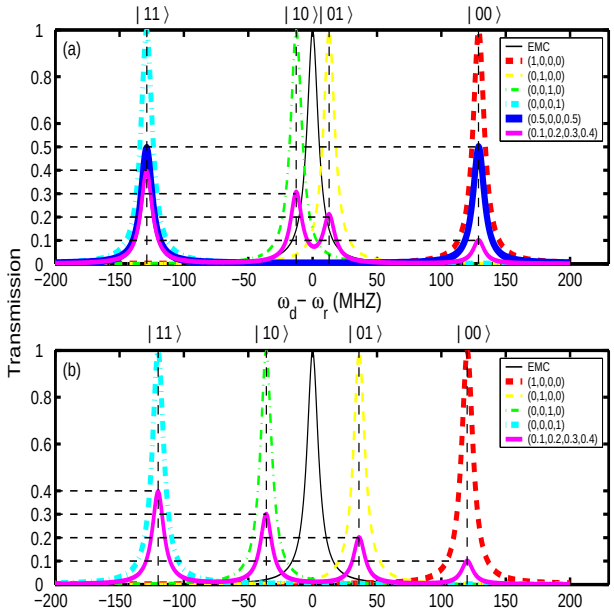

FIG. 3: (Color online) (a). Cavity transmission versus the probe detuning $\omega_d - \omega_r$ for certain selected two-qubit states with $|\alpha_1|^2 = 1$, $|\alpha_2|^2 = 1$, $|\alpha_3|^2 = 1$, $|\alpha_4|^2 = 1$, $(|\alpha_1|^2, |\alpha_2|^2, |\alpha_3|^2, |\alpha_4|^2) = (0.5, 0, 0, 0.5)$, and $(|\alpha_1|^2, |\alpha_2|^2, |\alpha_3|^2, |\alpha_4|^2) = (0.1, 0.2, 0.3, 0.4)$, respectively. For comparison, the empty cavity (EMC) transmission is also plotted in black line. Here, The parameters are $(\Gamma_1, \Gamma_2, \kappa, \gamma_{1,1}, \gamma_{1,2}) = 2\pi \times (-11.11, -9.11, 1.7, 0.02, 0.022,)$MHz [19, 23]. In (b) only the parameters Γ_1 and Γ_2 are modified as $\Gamma_1' = 1.05\Gamma_1$ and $\Gamma_2' = 0.85\Gamma_2$. In this case, the relative heights of the peaks are exactly equivalent to the corresponding probabilities of the single basis states superposed in the measured superposition state.

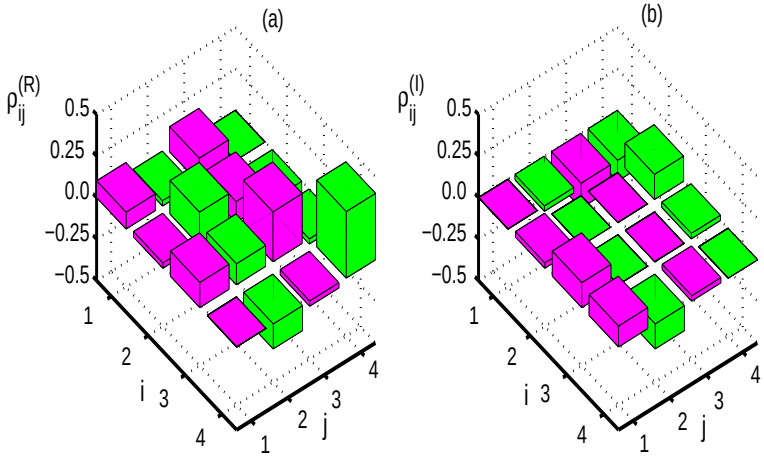

FIG. 4: (Color online) Schematic representations of the density matrix ρ_2 for a two-qubit state. The real $\rho_{ij}^{(R)}$ and imaginary $\rho_{ij}^{(I)}$ parts $(i, j = 1, 2, 3, 4)$ of the density matrix elements in the complete bases are plotted in (a) and (b), respectively.

Tables

TABLE I: The operational combinations before the QND measurements to determine the parameters for tomographically reconstructing a two-qubit state. The subscript "$1(2)$" of U is labeled for the operation of qubit $1(2)$.

quantum operation W	determined parameters
no	$r_{00}, r_{zz}, r_{0z}, r_{z0}$
$U_{\rm FF}U_{x_1}$	$r_{00}, r_{xy}, r_{yz}, r_{zx}$
$U_{\rm FF}U_{y_1}$	$r_{00}, r_{yx}, r_{zy}, r_{xz}$
$U_{\rm FF}U_{z_1}$	$r_{00}, r_{xx}, r_{yy}, r_{zz}$
$U_{y_1}U_{z_1}U_{\rm FF}$	$r_{00}, r_{0x}, r_{y0}, r_{yx}$
$U_{y_2}U_{z_2}U_{\rm FF}$	$r_{00}, r_{x0}, r_{0y}, r_{xy}$